Discover Water

Research

Functionalized graphitic carbon nitride as adsorbent for the removal of arsenic and lead from groundwater

Damian C. Onwudiwe[1,2] · Naledi H. Seheri[1,2] · Nnenesi A. Kgabi[3,4] · Dipti R. Sahu[5]

Received: 27 December 2023 / Accepted: 11 June 2024
Published online: 20 June 2024

Abstract
Water pollution caused by highly toxic arsenic (As) and lead (Pb) poses a serious threat to water quality. Hence, the development of materials for their effective removal from water continues to attract research attention. The present study reports functionalized graphitic carbon nitride nanosheets (GCN) as a green and low-cost adsorbent for the removal of As and Pb from polluted water. The adsorbent was prepared through the protonation and hydroxyl and cyano functionalized graphitic carbon nitride to form H/GCN and OH/CN-GCN respectively. Characterization techniques including Fourier transform infrared (FTIR), X-ray diffraction, and scanning electron microscopy were respectively used to study functional groups, structure, and morphology of the adsorbents. The adsorption study showed that modification of GCN with $^{-}$OH and CN^{-} ions in OH/CN-GCN, increased the density of negative charges on the functionalized surface, which also enhances the attraction of the positively charged ions. This may be responsible for the improved removal of As and Pb from wastewater compared to H/GCN. Isotherm studies on the adsorption behavior of OH/CN-GCN suggest that Langmuir isotherm model corroborates with the As adsorption. Therefore, indicating that the removal of As via its adsorption onto OH/CN-GCN is a surface phenomenon. However, the adsorption of Pb could be described as mainly a multilayer adsorption process, based on its R^2 value. It is proposed that the $^{-}$OH and CN^{-} groups on the tri-s-triazine units of GCN nanosheets may be responsible for the adsorption process. The prepared materials are promising adsorbents that nay find useful applications in wastewater treatment plants involving advanced oxidation processes.

Keywords Wastewater · Nanoadsorbents · Toxic metals · Graphitic carbon nitride · Isotherm

1 Introduction

Rapid industrialization and increasing population growth have severely impacted the environment, particularly the water sources, thus affecting water quality. Many industries across the globe are considered the primary source of harmful material released into the water sources leading to severe ecological imbalance and negative impact on animals and human health [1–4]. Hence, there is an increased global concern about heavy metal pollution in surface

✉ Damian C. Onwudiwe, Damian.Onwudiwe@nwu.ac.za; ✉ Nnenesi A. Kgabi, Nnenesi.Kgabi@nwu.ac.za; Naledi H. Seheri, naledi.seher@nwu.ac.za; Dipti R. Sahu, dsahu@nust.na | [1]Material Science Innovation and Modelling (MaSIM) Research Focus Area, Faculty of Natural and Agricultural Sciences, North-West University, Mafikeng Campus, Private Bag X2046, Mmabatho 2735, South Africa. [2]Department of Chemistry, School of Physical and Chemical Sciences, Faculty of Natural and Agricultural Sciences, North-West University, Mafikeng Campus, Private Bag X2046, Mmabatho 2735, South Africa. [3]Centre for Environmental Management, University of the Free State, Bloemfontein, South Africa. [4]Unit for Environmental Science and Management, North-West University, Potchefstroom, South Africa. [5]Department of Biology, Chemistry and Physics, School of Natural and Applied Sciences, Namibia University of Science and Technology, Private Bag 13388, Windhoek, Namibia.

water and groundwater sources. This pollution is attributed mainly to industrial activities such as mining, manufacturing, and power generation [5–7].

The increasing severity of heavy metal pollution is estimated to surge significantly in the coming decades because of climate change [8, 9]. The four most common heavy metals of interest to human health include Lead (Pb), cadmium (Cd), mercury (Hg), and Arsenic (As), with arsenic considered to be the most hazardous heavy metal released into the environment [10]. The main concern regarding these heavy metals is their inability to be metabolized within the body, which can result in harmful effects such as disrupting the body's nervous and defense systems and causing cancer [11].

Lead and arsenic cannot be converted into other forms in the body [12], hence, once absorbed, they are distributed to different organs. Therefore, increased intake of arsenic (As) from food and potable water can result in long-term human health effects such as arsenicosis, skin cancers, internal organ cancers, and many other ailments. Similarly, water sources contaminated with lead (Pb) may have an adverse case of osteoporosis [13].

Exposure to Pb can have a substantial effect on most organs and systems including the reproductive and nervous systems within the human body [14]. It is a naturally occurring element in the earth's crust with distinctive characteristics such as high malleability, softness, low melting point, and ductility [14]. However, these properties also make it a severe threat to human health. Exposure to lead has been linked to high blood pressure, kidney problems, and reproductive health issues in adults [15]. It can irreversibly damage mental and physical development in children, and those under the age of six are vulnerable to this metal's harmful effects [16, 17]. Its exposure to children even at low concentrations can cause adverse health effects such as learning difficulties, hearing defects, behavioural issues, and hyperactivity [18].

Various communities in different countries are exposed to higher arsenic levels through arsenic-rich groundwater intake. An increase in the pre-eminent levels of arsenic in groundwater sources has been adequately published in several countries, and it is estimated that other new areas with a higher concentration of this toxic metal are continuously being discovered in different regions across the globe [19, 20]. Conversely, lead is widely recognized as a prevailing environmental toxin because it is not biodegradable, and its toxic properties have been extensively researched [12]. This metal and its by-products are discharged into the air, soil, and waterways due to various industrial processes such as production of explosives and paint [18].

There has been a significant focus on eliminating lead and arsenic from water [21, 22]. The most prevalent toxic inorganic oxyanions forms of arsenic are trivalent arsenite (As III: H_3AsO_3 and $H_2AsO_3^-$) and pentavalent arsenate (As V: $H_2AsO_4^-$, $HAsO_4^{2-}$, and AsO_4^{3-}) that are present in terrestrial and water sources [23, 24]. These two inorganic forms of arsenic are considered to be 60 times more toxic, with As(III) existing mainly in a reducing environment, whereas As(V) occurs predominantly in an oxidizing environment [25, 26]. Lead is naturally present as lead (Pb^{2+}) sulphide or as a complex ore of lead and zinc sulphide [18].

Various technologies, such as membrane filtration, ion exchange, cementation, electrodialysis, photocatalytic degradation, electrolysis, and adsorption, have been established as methods to eliminate these heavy metals from water [27–29]. However, some of these methods are highly expensive, inefficient, and have complex procedures [30]. Among them, adsorption is considered the most widely used owing to its simple process, high efficiency, cost-effectiveness, and higher regeneration ability [2, 11]. Compared to other methods, the method is commendable due to its low operation cost and less sullying effects during the extraction process of removing toxic metals. Various adsorbents, including activated carbon, metal oxides, biomaterials, polymer resins, and many others, have been used as adsorbents for removing toxic pollutants through adsorption process [13, 31].

The development of novel materials as adsorbents continues to attract research attention due to the need to improve the efficiency of the existing materials. Graphitic carbon nitride (GCN or g-CN) has recently been discovered as a potential material in wastewater remediation. It is considered the most stable allotrope of carbon nitride due to its non-toxic, cost-efficient, thermal (at about 600 °C), and chemical stability [32]. Graphitic carbon nitride is poorly soluble in water, diethyl ether or ethyl acetate, and acetone, and it does not react readily with weak acids and bases. The material can be used widely in various applications based on these properties. The tri-s-triazine form of this polymer contains nitrogen functional groups ($-NH_2$, –NH, –N=) that act as active binding sites to bond with metal ions via complexation and have high removal efficiency compared to the pristine form. In addition, the tri-s-triazine polymer is a semiconductor with a medium band gap of 2.7 eV, and it absorbs at a good visible light region of around 450–460 nm [33]. The low efficiency of the pristine compound may be attributed to the presence of a few functional groups on the surface and their hydrophobic property [34]. This could be addressed by the surface modification of graphitic carbon nitride by improved functionalization of its surface chemistry.

Different methods have been used to improve the efficiency of GCN such as coupling with functional materials [35], doping with different elements to tune the light-responsive range of GCN and improve the charge separation process for photocatalysis [36], and copolymerization [37]. Although these modification approaches have been reported to improve the performance of GCN, they entail the introduction of secondary materials. Hence, in most cases they are not economical and require a long and painstaking synthesis process. In this study, covalent functionalization of the surface of graphic carbon nitride was carried out, through a simple use of acid and base, and was used as an adsorbent to remove arsenic and lead from wastewater.

Real water samples were obtained from Groot Marico Biosphere Reserve, one of the UNESCO-protected environments that are secluded from anthropological activities, in the North West Province of South Africa, hence it is a good location for sampling to study the efficiency of the synthesized GCN and also to show that pollution of groundwater by heavy metals is possible in secluded areas. The samples were collected from two different streams: Kaaloog se Loop before Komkrans (stream 1) and Rietspruit (stream 2), and the effect of process variables and the kinetic study were studied.

2 Experimental procedure

2.1 Synthesis of surface-functionalized graphitic carbon nitride

Two methods were employed to prepare the surface-functionalized graphitic carbon nitride, which involved the use of a strong acid and a strong base. In both cases, melamine was used as the precursor, and high-temperature calcination was devised.

2.1.1 Synthesis of protonated graphitic carbon nitride (H/GCN)

A method reported by Wee-Jun Ong, et al. [38] was employed to prepare the protonated GCN. About 20 g of melamine was placed in a ceramic crucible with a lid and closed to minimize the sublimation of the precursor. The melamine was then heated to 550 °C and maintained for 4 h in a furnace. The sample was allowed to cool to room temperature, and the bright yellowish product obtained was ground into a fine powder. Thereafter, the GCN was exfoliated by the treatment with 100 mL of 32% HCl and ultrasonication of the solution for 1 h. The exfoliated GCN was protonated by vigorously stirring the GCN-acid suspension for 4 h. The mixture was then filtered and washed several times with deionized water until a neutral pH was attained. The obtained H/GCN was dried in an oven for 24 h at 50 °C.

2.1.2 Synthesis of hydroxyl and cyano functionalized graphitic carbon nitride

Hydroxyl and cyano functionalized graphitic carbon nitride followed a method described by Ghazy et al. [39]. About 1.5 g of the pristine GCN was ground with 0.45 g of anhydrous potassium hydroxide using mortar. The homogenized product was placed in a ceramic boat and transferred to a muffle furnace at 700 °C for 2 min. Thereafter, the ceramic boat was quickly removed from the furnace and then allowed to cool down to room temperature. The resulting powder (pale brown) was ground to finer particles and rinsed thoroughly with distilled water to a neutral pH before drying in vacuo at 60 °C. The synthesis procedure has been provided in Scheme 1.

2.2 Preparation of synthetic wastewater

The metal ions solutions were prepared in binary solution using arsenic nitrate and lead nitrate salts in distilled water. The dilution of solutions was done to the required concentration and analysed using Inductively Coupled Plasma Optical Emission spectroscopy (ICP-OES).

2.3 Collection and analysis of real water samples

Real water samples were obtained from Groot Marico Biosphere Reserve in the North-West province of South Africa. The Biosphere Reserve is situated between 25°29′18″S and 26°23′47″E, and covers an area of 36.17 km^2. A batch equilibrium experiment was conducted to determine the adsorptive capacity of the functionalized GCN on the removal of heavy metals from water. The first study was the effect of the pH of solution to ascertain the optimum pH suitable for the adsorption

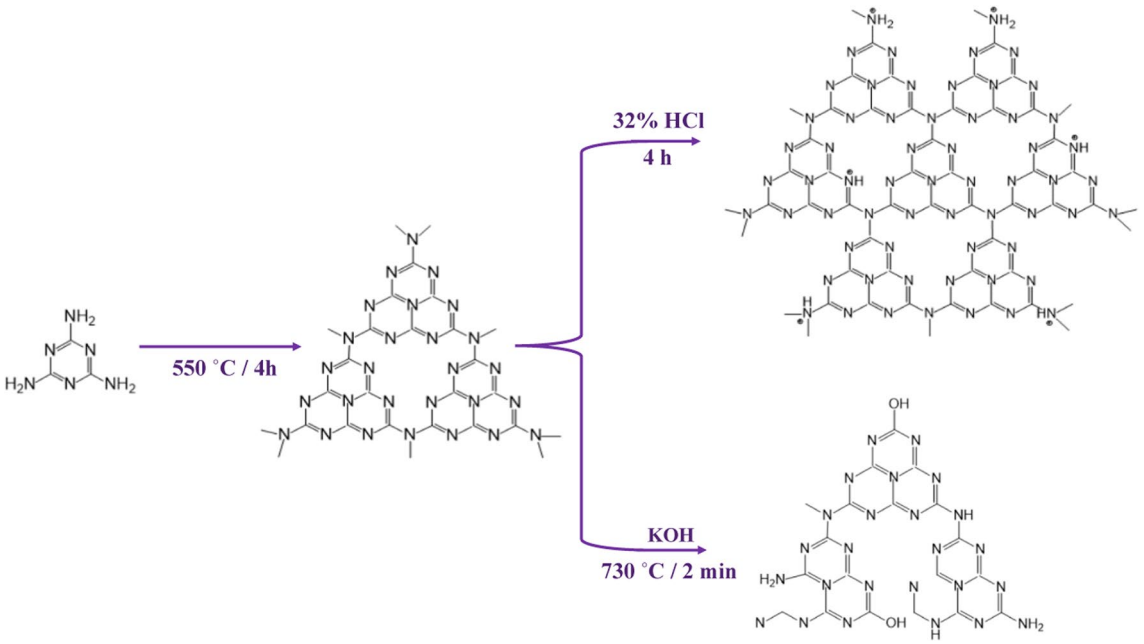

Scheme 1 The synthesis route for the preparation of functionalized GCN

process. A solution of 0.1 M NaOH or 0.1 M HCl was used for the pH adjustment. The results obtained from the ICP-OES analysis of the surface water from two different points are presented in tabular form.

2.4 Removal of heavy metals from wastewater by adsorption process

About 0.1 g of the functionalized GCN was added to a 50 mL solution of arsenic (100 mg/L) in 100 mL sterile plastic bottles. The real water sample contained 5.36; 5.46 mg/L and 7.3; 6.01 mg/L of As and Pb, from streams 1 and 2 respectively.

Thereafter, the water sample bottles were placed in a NUVE ST30 thermostatic shaker and operated for 24 h at 200 rpm. After the contact period of reaction, filtration of the samples was carried out using 0.45 µm pore size syringe filter. The analysis of the filtrate was done using ICP-OES for the determination of the residual concentration of the pollutant. This procedure was repeated to study the effect of the weight of the adsorbent, pollutants' concentration, solution temperature, and pH on the amount of pollutant adsorbed. The weight of the adsorbent loading was varied from 0.01 g to 0.15 g, while the concentration effect was studied by changing the concentration of the pollutants from 2 mg/L to 50 mg/L. The concentration of the real mine water was unchanged and was used as received from the sampling sites, except in the study of the isotherm. The study involving the effect of temperature on the adsorption process was carried out in the 25 °C to 45 °C temperature range. The mass of the adsorbent used was maintained at 0.1 g as the pollutant's concentration varied in both synthetic and real sample water for the isotherm study.

The percentage removal efficiency of the adsorbent R_t was determined using Eq. 1, while the equilibrium uptake q_e in mg/g was evaluated from Eq. 2.

$$R_t = \frac{C_o - C_e}{C_o}.100 \tag{1}$$

$$q_e = \frac{C_o - C_e}{m}.V \tag{2}$$

where C_o is the pollutants' initial concentration in (mg/L), C_e is the pollutant's concentration at equilibrium in (mg/L), m is the adsorbent's mass in (g), and V is the volume of the sample solution in (L).

Langmuir and Freundlich's models were used for the interpretation of the equilibrium isotherm data. Equation 3 presents the linear forms of the Langmuir adsorption isotherm, while Eq. 4 shows the Freundlich isotherm.

$$\frac{C_e}{q_e} = \frac{1}{q_o{}^b} + \frac{C_e}{q_o} \tag{3}$$

$$\mathrm{Log}q_e = \log K_F + \frac{1}{n}\log C_e \tag{4}$$

where b is the Langmuir constant, q_o is the Langmuir maximum adsorption capacity, K_F and n are the Freundlich parameters that are related to the adsorption capacity and intensity, respectively.

2.5 Characterization of GCN

The functionalized GCN was characterized using D8 Advance X-ray diffractometer by Bruker (Billerica, MA, USA) using Cu Kα radiation and in the 2θ range between 20 and 40°. The morphology was studied using scanning electron microscope (SEM) operated on a FE-SEM FEI 430 Nova NanoSEM system) (JSM-7600F). FTIR analysis was carried out on a Cary 670 FTIR spectrometer and the spectra were measured in the range of 400 to 4000 cm^{-1}.

3 Results and discussion

3.1 Structural and morphological characterizations of the GCN

The powder X-ray diffraction patterns of the pristine and the functionalized carbon nitride samples are shown in Fig. 1. The reflections from the (002) crystal plane attributed to the interlayer stacking of aromatic rings appeared around 2θ = ~ 27.5° [40–43]. This characteristic peak has a typical interlayer spacing of 0.325 nm [44, 45]. A close observation of this (002) plane reveals a slight increase in broadness with an increase in functionalization and in the peak positions as well as full width at half maximum (FWHM). The increase in broadness and lower intensity indicates the presence of smaller crystalline domains [46]. The position of this reflection shifted slightly towards the 2θ = 0, indicating a slight increase in interlayer spacing [47]. Higher angles have been reported to relate to smaller interplanar distances, and the existence of the peak at this position clearly confirms the crystalline nature of GCN in the 3 samples.

The crystallite size of the samples was estimated using Scherrer formula, presented in (5)

$$\mathrm{D} = \mathrm{K}\lambda/\beta\cos\theta \tag{5}$$

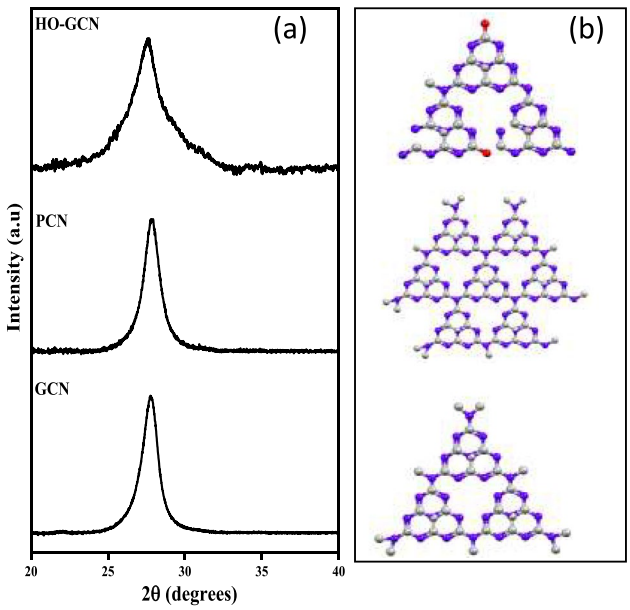

Fig. 1 **a** XRD pattern of GCN, H/GCN and HO/CN-GCN. **b** corresponding structure of GCN, H/GCN and HO/CN-GCN

where D = crystallite size (nm), K = Scherrer constant (0.94), λ = radiation wavelength, which is 1.5418 Å, and β is the full width of (002) crystallite peak at half maximum.

The FTIR spectra of the pristine and functionalized samples (Fig. 2) are typical structures of GCN. The peaks in the range of 1500–1700 cm^{-1} and 1200–1480 cm^{-1} correspond to the characteristic ring stretching vibration of C=N and C–N heterocycles. The presence of tri-s-triazine (heptazine) subunits is indicated by the number and shape of the bands, which is also confirmed by the doublet at 1580 cm^{-1} [48]. The ring system in graphitic carbon nitride is linked by –NH– groups, and this is shown by the vibrational bands around 1200–1400 cm^{-1}. This region is indicative of the C–NH–C units in the precursor compound [49] and has been attributed to the manifestation of the tertiary amine (C–NH–C) fragments [50, 51]. Furthermore, it confirms the formation of carbon nitride polymer that is in a more condensed nature. Structurally, the C–N stretching bands of tertiary amines are associated with weak to medium intensity bands, ascribed to the absence of polarity in the C–N bond [48].

SEM images, presented in Fig. 3 reveal corrugated surface structure with twisted sheets, typical of graphitic carbon nitride [45]. Higher crystallinity could be observed for the pristine carbon nitride (Fig. 3a) than those of the functionalized samples, which showed well-interlocked sheets with fewer available spaces. Moreover, the pristine sample has larger sheets with higher exfoliation than the functionalized samples (Fig. 3a and b). It also presents a more delicate and brittle structure than the functionalized ones and may be a result of less surface activity taking place on the sheets. Figure 3b and c indicate a decrease in the particle size with increasing surface functionalization and the smallest particle size of carbon nitride is obtained.

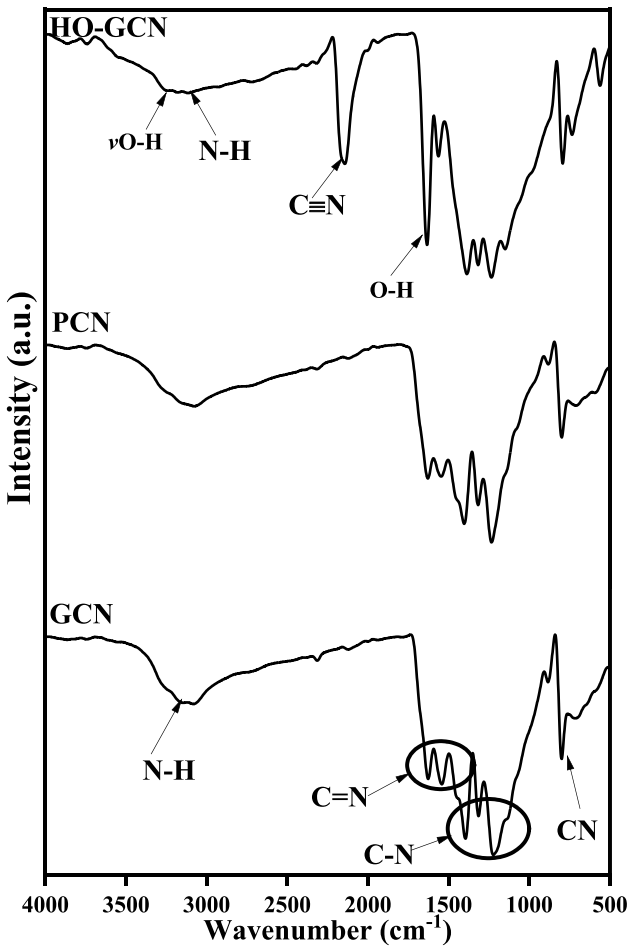

Fig. 2 FTIR plot of GCN, H/GCN and OH/CN-GCN

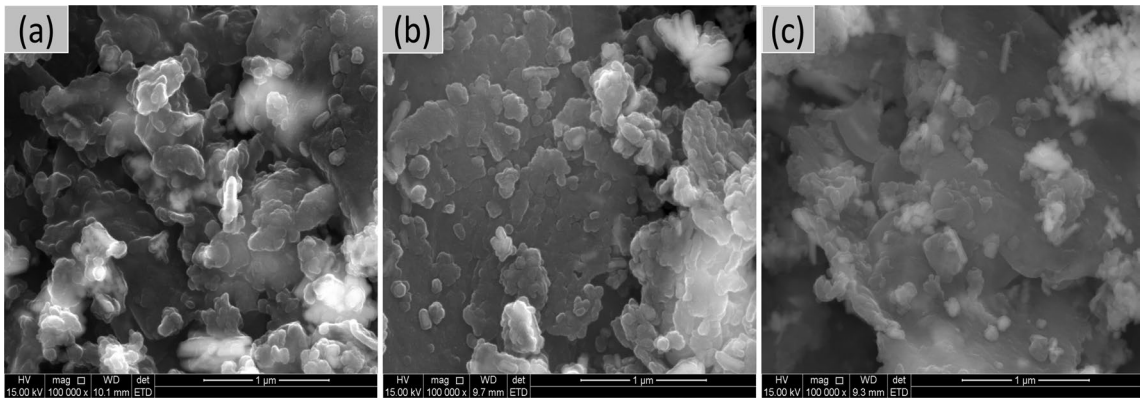

Fig. 3 SEM micrographs of **a** pristine GCN, **b** H/GCN, and **c** OH/CN-GCN

3.2 Adsorptive performance of the functionalised graphitic carbon nitride

3.2.1 Effect of solution pH on the adsorption of As and Pb ions

In adsorption studies, the pH of the solution is a very important factor because it affects the ionic species present in both the adsorbent and adsorbate [52]. The adsorption of arsenic (As) and lead (Pb) onto the surface of both functionalized graphitic carbon nitride (H-GCN and OH/CN-GCN) was found to be highly dependent on pH. The optimal pH was 5.0 and 4.0 for As using OH/CN-GCN and H-GCN respectively, while the adsorption of Pb ions was optimal at pH 4 and 7.0 using OH/CN-GCN and H-GCN, as shown in Fig. 4a and b respectively. This implies that the adsorption of both metal ions occurs mostly in the acidic range. The domination of hydroxonium ions (H_3O^+) in the acidic medium contends with the metal ions for the active sites on both functionalized GCN. Hence, an increase in the pH value, increases the adsorption process due to a reduction in the competition from hydroxonium ions [53]. The percentage removal remains comparably constant at pH 5.0 for As and 4.0 for Pb using OH/CN-GCN, which is the most efficient adsorbent in this study. In addition, pH influences the solubility of the metal ions as a result of the concentration of counter ions on the adsorbent's functional groups and the extent of ionization of the adsorbate during the reaction [54].

The modification of GCN with ^{-}OH and CN^{-} ions increased the density of negative charges on the functionalized surface, which also enhances the attraction of the positively charged ions. This results in the increase of As and Pb removal

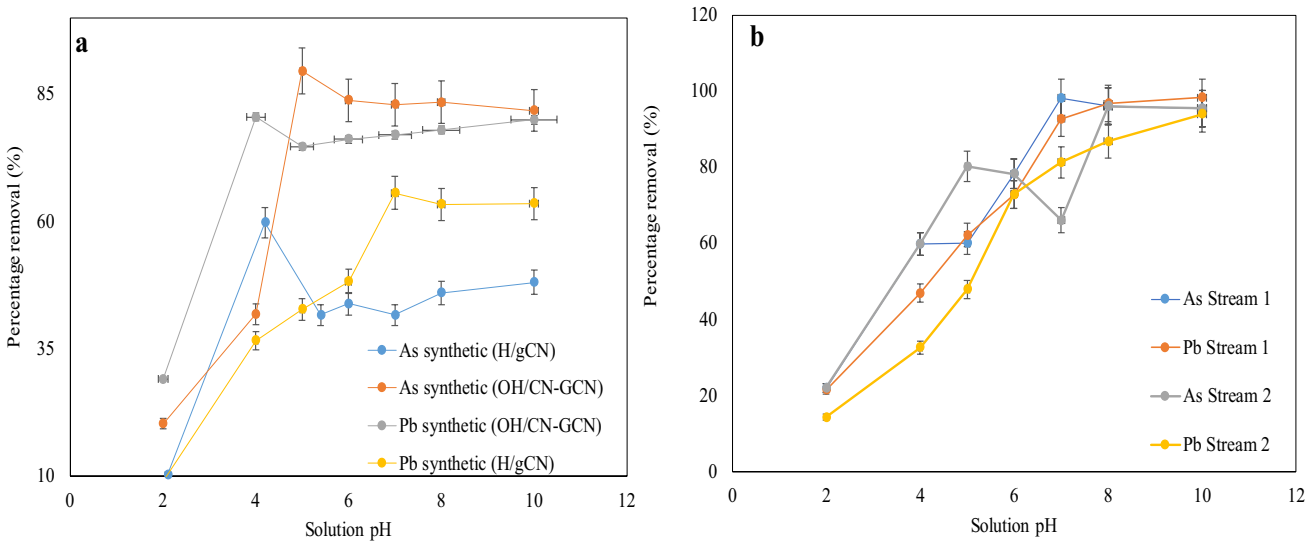

Fig. 4 Effect of solution pH on the adsorption of As and Pb from synthetic water using **a** OH/CN-GCN and **b** H-GCN (temp. 25, 24 h duration, 50 mg/L initial conc., and adsorbent weight of 0.1 g)

from wastewater [55]. However, there might be the involvement of multiple mechanisms in the sorption at high pH values beyond the optimum pH of 7, and that could result to lower removal of the metal ions below the expected range[56, 57]. In samples obtained from streams 1 and 2, the optimal pH for As and Pb removal was found around the neutral range (Fig. 4b). Overall, the removal capacity achieved with the use of OH/CN-GCN was higher than H/GCN in both the synthetic and real water samples. This might be attributed to presence of negative charges created by the OH group on the surface of GCN, therefore, OH/CN-GCN was used for all subsequent adsorption studies.

3.2.2 Effect of adsorbent's dosage on the adsorption of As and Pb ions

The effect of OH/CN-GCN dosage on the adsorption of As and Pb ions was studied over a weight gradient and the results are presented in Fig. 5. An increase in the amount of dosage from 0.01 to 0.15 g, also increased the percentage removal of As and Pb from 15.2 to 96.4% and 12.0 to 88.4% respectively. This indicates that the increase in the adsorption of both metal ions on the adsorbent increases with an increase in the amount of dosage. However, the removal capacity remained almost the same after the adsorbent dose of 0.1 g. This could be ascribed to the intercellular distance reduction of the OH/CN-GCN sites brought about by the complexed ion species, thereby resulting in the shielding of binding sites from the unbonded metal ions [58]. The enhanced surface area of OH/CN-GCN upon modification might have created an increased availability of binding sites capable of complexing the specific metal ions [59]. According to Musumba et al. [60] the variance in the adsorption of metals is correlated to the susceptibility of their ions to hydration. Hence, the enhanced adsorption of As might be a result of the difference in the hydrated ionic radius. The overall removal efficiency achieved in both As and Pb using the OH/CN-GCN is comparable with previously reported studies [53, 55].

3.2.3 Adsorption isotherms

Experimental data from the adsorption process could either be interpreted using newly simulated models or with existing models. According to Srivastava et al. [61], the amount of adsorbate on the surface of the adsorbent (due to its pressure or concentration at a stable temperature) is known as an isotherm. This describes where the adsorption process is typically most noticeable. To guarantee the similarities and differences of many materials, the amount of adsorbate adsorbed is typically stabilized by the adsorbent weight. Consequently, the adsorption experimental data in this study were described using the two widely used isotherm mathematical models including the Langmuir and Freundlich isotherm models.

The Langmuir model expresses a single layer adsorption process that takes place on a definite site of a homogeneous adsorbent. Therefore, the adsorption energy of each active site on the surface of the adsorbent is related. In contrast, the Freundlich adsorption model describes a multilayer adsorption process that occurs on heterogeneous sites of the adsorbent, and the adsorption sites possess varying affinities toward the adsorbate [62]. A temperature range between 25 and 45 °C was explored to assess the dependence of the process on temperature in As and Pb sorption onto OH/CN-GCN using synthetic water. Figure 6a and b present the adsorptive behaviour of As and the fitted curve for Langmuir model, while the change in Pb adsorption and the fitted Freundlich models are presented in Fig. 7a and b at different temperature ranges.

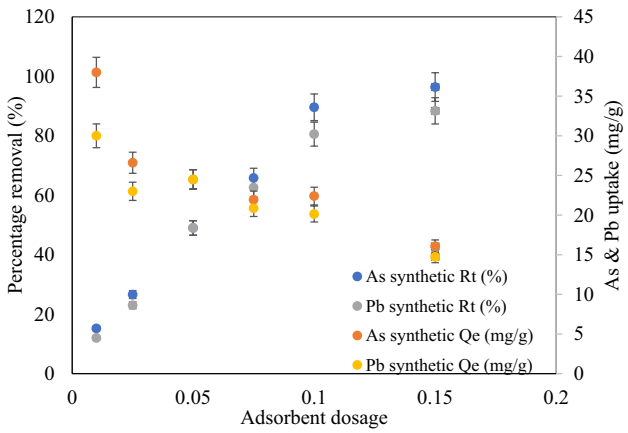

Fig. 5 Effect of adsorbent dosage on As and Pb adsorption (synthetic water; 50 mg L^{-1} initial conc. and pH of 5.0 (As); 6.0 (Pb), Temp. 25 °C, 24 h duration)

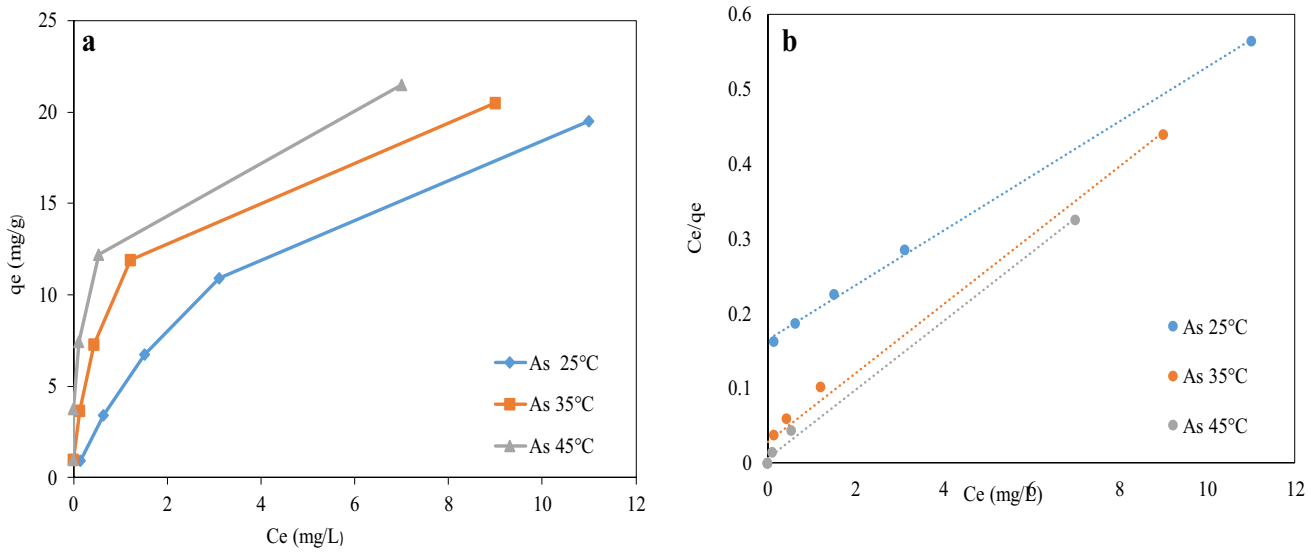

Fig. 6 **a** The isotherms graph for the sorption of As onto OH/CN-GCN (pH 5.0, 24 h duration, 2 mg/L to 50 mg/L initial conc. and 0.1 g sorbent mass) and **b** fitted curve for Langmuir model.

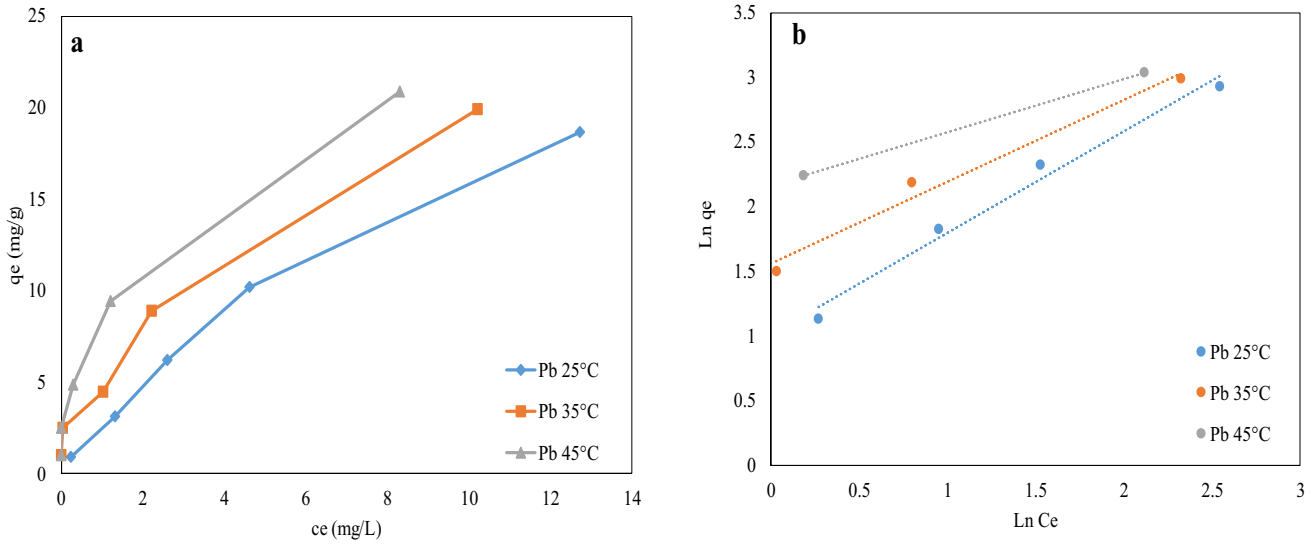

Fig. 7 **a** The isotherms for Pb sorption onto OH/CN-GCN and **b** Fitted Freundlich models (pH 6, 24 h duration, 2 mg/L to 50 mg/L initial conc. and 0.1 g sorbent mass)

A positive change in equilibrium concentration resulted in an increase in the equilibrium uptake of As and Pb, and a direct relationship could be observed in temperature gradient and adsorption capacities in both cases. This indicated that As and Pb sorption onto OH/CN-GCN are temperature-dependent processes [63]. The increased sorption at higher temperatures might be due to the reduction in the width of the boundary layer that surrounds the OH/CN-GCN [64]. The molecules' rapid movement with increase in temperature might also be responsible for the increase in adsorption capacities [64].

R^2 values and the plotted values indicated that the Langmuir isotherm model corroborates with the experimental data of As in comparison to the Freundlich model, indicating that the adsorption of As on to OH/CN-GCN occurred at a particular adsorbent site. However, based on the R^2 values as well as all the plotted values, the adsorption of Pb could be described as mainly a multilayer adsorption process. Furthermore, the results indicate that q_e, which determines the ability of the adsorbent's monolayer and the Freundlich isotherm's estimated K_F values, increased with increase in the temperature, while the reverse was the case for the Langmuir constant *b* (Table 1). Hence, confirms an increased sorption of both metals at higher process temperature**.**

Table 1 Summary of equilibrium isotherms parameters of As and Pb sorption unto OH/CN-GCN

Temperature (°C)	*Arsenic (As)*					
	Langmuir isotherm parameters			Freundlich isotherm parameters		
	q_m (mg/g)	*b* (L/mg)	R^2	K_F (L/g)	*1/n*	R^2
25	22.73	5.01	0.999	3.33	0.74	0.7968
35	23.30	6.84	0.994	5.98	0.38	0.7176
45	29.79	16.30	0.999	4.52	0.23	0.8217
Temperature (°C)	*Lead (Pb)*					
	Langmuir isotherm parameters			Freundlich isotherm parameters		
	q_m (mg/g)	*b* (L/mg)	R^2	K_F (L/g)	*1/n*	R^2
25	13.20	0.31	0.899	2.76	0.78	0.998
35	15.70	0.62	0.812	4.77	0.63	0.998
45	22.00	0.63	0.965	8.72	0.41	1.000

Table 2 Characterization of surface water concentration from two different points in Groot Marico Biosphere Reserve, South Africa

Elements	Stream 1 (mg/L)	Stream 2 (mg/L)
pH	5.23	6.20
K	937.88	1170.22
Ca	1124.25	1390.20
Sc	1.34	1.70
Ti	0.77	1.35
V	0.09	0.10
Cr	1.51	1.96
Mn	0.05	0.07
Fe	77.22	104.30
Co	0.03	0.03
Ni	0.00	0.00
Cu	0.12	0.15
Zn	0.63	0.79
As	5.36	5.46
Se	0.32	0.45
Br	8.65	11.68
Pb	7.30	6.01

3.3 Marico bioreserve surface water treatment using functionalized graphitic carbon nitride (OH/CN-GCN)

The Marico Biosphere Reserve surface water, sampled in two different stream points, was analysed, and the results are presented in Table 2. The adsorption experiment involving these two water samples was performed with a pH adjustment to 7.0 since the optimal removal of As and Pb in the stream water samples was achieved at the neutral pH. In addition, the pH of the stream water sample was measured and presented in Table 2. It is notable that the adsorption of some metal ions might be limited without pH adjustment, or due to other constituents competing for the available active sites on the surface of OH/CN-GCN [65]. However, the recorded pH seems favourable for the removal of other metal ions in the water samples and the treated water might be rendered fit for consumption.

The total removal of Mn, Co, Cu, Zn, Se, Sc, Ti, and V simultaneously in addition to the removal of As, Pb, was observed in both samples from streams 1 and 2 (Fig. 8). OH/CN-GCN is a hydrophilic adsorbent, therefore most metal ions in its vicinity could easily attach to the material in the hydrated ions' form of [62]. In addition, large hydration radius of the

metal ions easily react with water molecules and most of the metal ions present in both samples have higher hydrated ionic radius especially Pb and As [66]. The amount of adsorbent used might also be responsible for an efficient removal of these metal ions due to the availability of effective adsorption sites in the medium as a result of the higher adsorbent dose [67].

Although, a substantial amount of K, Ca, Br, Cr, Pb, Ni, As, S metal ions was removed in both water samples, a lower adsorption indicates that OH/CN-GCN has a low affinity for these metals compared to the other metals present in the samples [68]. In some cases, when the valency of the metal ions are the same, then the adsorption of the metal with a larger hydrated ionic radius will be favoured [69]. It is not broad enough to assess the removal rate of an individual toxic metal ions in solution; therefore, solution containing multiple toxic metal could assess the affinity of toxic metal ions on the OH/CN-GCN adsorbent. A very low adsorption capacities was also observed for the removal of Fe from stream 1 and 2, which might be due to the adsorption of Fe, which usually occurs between pH 2–4. Hence, the presence of trivalent iron (Fe^{3+}) is suspected [70, 71].

Attractively, the OH/CN-GCN presents efficient As and Pb removal in both samples, and the level of As, Pb, Mn, Co, Cu, Zn, Se, Sc, Ti, V contents are below the drinking water standard recommended by the World Health Organization, especially for As and Pb [72, 73]. The experimental studies suggest that the OH/CN-GCN could be a potential candidate for the removal of toxic metal ions from the water samples of similar matrices.

3.4 Comparative evaluation of various nano-adsorbents for As & Pb removal

The adsorption efficiency of the investigated functionalized graphitic carbon nitride nanosheets in removing Pb and As has been compared with different graphitic carbon nitride-based nanoadorbents and other nanomaterials from the literature, as shown in Table 3. The high removal efficiency in this study is attributed to the special use of the acid and a base. Acid treatment protonated the surface of graphitic carbon nitride, while base treatment introduced both ^{-}OH and CN^{-} ions, enhancing adsorption efficiency through the presence of multiple functional groups.

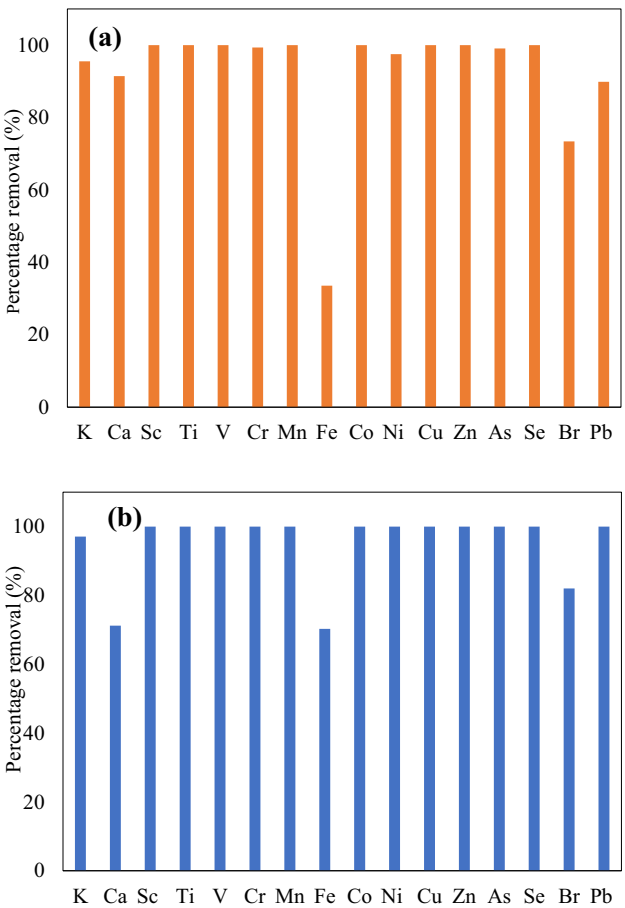

Fig. 8 Adsorptive performance of OH/CN-GCN in surface water treatment from **a** Stream 1 **b** stream 2 (temp. 25 °C, duration 24 h, dosage 0.2 g)

Table 3 Comparative evaluation of various nano-adsorbents for As & Pb removal

Adsorbent	Adorbate	pH	Contact time	Percentage% removal	Refs.
OH/CN-GCN	As(V) Pb	4 4	24 h 24 h	88.4 96.4	This work
g-C_3N_4 g-C_3N_4/Fe (g-nZVI)	Pb(II) Pb(II)	5.5	30 min 15 min	8 ~80	[74]
HAP-biopolymer nanocomposites: HAP-CTS HAP-biopolymer nanocomposites: HAP-GEL	As(V) Pb(II)	6.9 6.3	6 min 5 min	91 85	[75]
Clay and nanoclay ceramic granules	Pb As	5–8	24 h	80–88 18–22	[76]
Magnetic Nanoparticles onion peel MNp-OP	As(III) & As(V)	5.63		55–61	[77]
Fe_3O_4 nanoparticles (Fe_3O_4 NPs) magnetic composite Fe_3O_4@SiO_2	As(V)	> 7 4.0	4 h 22 h	60 80	[78]
carboxymethyl cellulose-immobilized Fe3O4 nanoparticles CMC-Fe_3O_4	Pb(II)	2–6		68.4	[79]
magnetite nanocomposites : coated sand	As(V)	2–7	30 min		[80, 81]
Fe_3O_4-nonoxidative graphene/CNT (M-G/C)	As (III) As(V)	7.0		91 78	[82]
Magnetic Fe_3O_4/Douglas fir biochar composites (MBC)	As(III)	2–6		65	[83]

4 Conclusion

In the present work, an environmentally friendly and low-cost adsorbent of functionalized GCN nanosheets was developed using both acid and base. While the acid treatment resulted in the protonation of the graphitic carbon nitride's surface, the base afforded the surface functionalization with both $^{-}$OH and CN^{-} ions, thereby leading to higher adsorption efficiency due to the multiple functional groups. At the optimum pH of 5, an increase in the amount of dosage from 0.01 to 0.15 g, increased the percentage removal of As and Pb from 15.2 to 96.4% and 12.0 to 88.4% respectively. In addition to the removal of the target metals, the simultaneous total removal of Mn, Co, Cu, Zn, Se, Sc, Ti, and V was observed in the real water samples obtained from Groot Marico Biosphere Reserve. The presented paper not only demonstrated a simple and environmentally friendly route to prepare porous GCN nanosheets with good adsorption property for Pb and As, but also showed the underlying mechanism for the adsorption process. However, the poor recoverability of the GCN over a long period of reuse is a potential limitations that could impede the practical applications of this material to groundwater treatment.

Acknowledgements The authors acknowledge support from the North-West University, South Africa and Groot Marico Biosphere Reserve Management, South Africa.

Author contributions DCO: conceptualization, investigation, methodology, writing—original draft preparation. NHS: methodology, formal analysis, writing—original draft preparation. NAK: Resources, writing—review and editing. DRS: resources, writing—review and editing.

Funding Open access funding provided by North-West University. This research was funded by the North-West University, South Africa.

Data availability Data will be made available on request.

Declarations

Competing interests The authors declare that there is no competing interests.

References

1. Mateo-Sagasta J, Zadeh SM, Turral H, Burke J. Water pollution from agriculture: a global review: executive summary. Rome: FAO; 2017.
2. Tripathy M, Padhiari S, Ghosh A, Hota G. Polyacrylonitrile support impregnated with amine-functionalized graphitic carbon nitride/magnetite composite nanofibers towards enhanced arsenic remediation: a mechanistic approach. J Colloid Interface Sci. 2023;640:890–907.
3. Mitra S, Chakraborty AJ, Tareq AM, Emran TB, Nainu F, Khusro A, Idris AM, Khandaker MU, Osman H, Alhumaydhi FA. Impact of heavy metals on the environment and human health: novel therapeutic insights to counter the toxicity. J King Saud Univ Sci. 2022;34:101865.
4. Fatoki JO, Badmus JA. Arsenic as an environmental and human health antagonist: a review of its toxicity and disease initiation. J Hazard Mater Adv. 2022;5:100052.
5. Ali H, Khan E, Ilahi I. Environmental chemistry and ecotoxicology of hazardous heavy metals: environmental persistence, toxicity, and bioaccumulation. J Chem. 2019;2019:6730305.
6. Briffa J, Sinagra E, Blundell R. Heavy metal pollution in the environment and their toxicological effects on humans. Heliyon. 2020;6(9):e04691.
7. Li P, Karunanidhi D, Subramani T, Srinivasamoorthy K. Sources and consequences of groundwater contamination. Arch Environ Contam Toxicol. 2021;80(1):1–10.
8. Amrose SE, Cherukumilli K, Wright NC. Chemical contamination of drinking water in resource-constrained settings: global prevalence and piloted mitigation strategies. Ann Rev Environ Resour. 2020;45:195–226.
9. Johnston J, Cushing L. Chemical exposures, health, and environmental justice in communities living on the fenceline of industry. Curr Environ Health Rep. 2020;7(1):48–57.
10. Mitra S, Chakraborty AJ, Tareq AM, Emran TB, Nainu F, Khusro A, Idris AM, Khandaker MU, Osman H, Alhumaydhi FA, et al. Impact of heavy metals on the environment and human health: novel therapeutic insights to counter the toxicity. J King Saud Univ Sci. 2022;34(3):101865.
11. Gupta A, Sharma V, Sharma K, Kumar V, Choudhary S, Mankotia P, Kumar B, Mishra H, Moulick A, Ekielski A, et al. A review of adsorbents for heavy metal decontamination: growing approach to wastewater treatment. Materials. 2021;14(16):4702.
12. Boskabady M, Marefati N, Farkhondeh T, Shakeri F, Farshbaf A, Boskabady MH. The effect of environmental lead exposure on human health and the contribution of inflammatory mechanisms, a review. Environ Int. 2018;120:404–20.
13. Soni R, Pal AK, Tripathi P, Lal JA, Kesari K, Tripathi V. An overview of nanoscale materials on the removal of wastewater contaminants. Appl Water Sci. 2020;10(8):189.
14. Huda BN, Wahyuni ET, Mudasir M. Eco-friendly immobilization of dithizone on coal bottom ash for the adsorption of lead(II) ion from water. Results Eng. 2021;10:100221.
15. Kokate S, Parasuraman K, Prakash H. Adsorptive removal of lead ion from water using banana stem scutcher generated in fiber extraction process. Results Eng. 2022;14:100439.
16. Wani AL, Ara A, Usmani JA. Lead toxicity: a review. Interdiscip Toxicol. 2016;8(2):55–64.
17. Zaidi R, Khan SU, Azam A, Farooqi IH. A study on effective adsorption of lead from an aqueous solution using copper oxide nanoparticles. IOP Conf Ser Mater Sci Eng. 2021;1058:012074.
18. Chowdhury IR, Chowdhury S, Mazumder MAJ, Al-Ahmed A. Removal of lead ions (Pb2+) from water and wastewater: a review on the low-cost adsorbents. Appl Water Sci. 2022;12(8):185.
19. Shaji E, Santosh M, Sarath K, Prakash P, Deepchand V. Divya BJGf: Arsenic contamination of groundwater: a global synopsis with focus on the Indian Peninsula. Geosci Front. 2021;12(3):101079.
20. Khosravi-Darani K, Rehman Y, Katsoyiannis IA, Kokkinos E, Zouboulis AI. Arsenic exposure via contaminated water and food sources. Water. 2022;14(12):1884.
21. Balali-Mood M, Naseri K, Tahergorabi Z, Khazdair MR, Sadeghi M. Toxic mechanisms of five heavy metals: mercury, lead, chromium, cadmium, and arsenic. Front Pharmacol. 2021;12:643972.
22. Velusamy S, Roy A, Sundaram S, Kumar Mallick T. A review on heavy metal ions and containing dyes removal through graphene oxide-based adsorption strategies for textile wastewater treatment. Chem Rec. 2021;21(7):1570–610.
23. Wang N, Ye Z, Huang L, Zhang C, Guo Y, Zhang W. Arsenic occurrence and cycling in the aquatic environment: a comparison between freshwater and seawater. Water. 2023;15(1):147.
24. Weidner E, Ciesielczyk F. Removal of hazardous oxyanions from the environment using metal-oxide-based materials. Materials. 2019;12(6):927.
25. Polya DA, Sparrenbom C, Datta S, Guo H. Groundwater arsenic biogeochemistry—key questions and use of tracers to understand arsenic-prone groundwater systems. Geosci Front. 2019;10:1635–41.
26. Tripathy M, Padhiari S, Kar S, Hota G, Ghosh AK. Hematite decorated functional porous graphitic carbon nitride binary nanohybrid: mechanistic insight into the formation and arsenic adsorption study. Appl Surf Sci. 2022;583:152443.
27. Carmona B, Abejón R. Innovative membrane technologies for the treatment of wastewater polluted with heavy metals: perspective of the potential of electrodialysis, membrane distillation, and forward osmosis from a bibliometric analysis. Membranes. 2023;13(4):385.
28. Ahmad A, Mohd-Setapar SH, Chuong CS, Khatoon A, Wani WA, Kumar R, Rafatullah M. Recent advances in new generation dye removal technologies: novel search for approaches to reprocess wastewater. RSC Adv. 2015;5(39):30801–18.
29. Collivignarelli MC, Abbà A, Miino MC, Damiani S. Treatments for color removal from wastewater: state of the art. J Environ Manage. 2019;236:727–45.
30. Guo S, Duan N, Dan Z, Xu F, Zhang C, Shi F, Gao W. Three-dimensional magnetic graphitic carbon nitride composites as high-performance adsorbent for removal Pb2+ from aqueous solution. J Taiwan Inst Chem Eng. 2018;89:169–82.

31. Sadegh H, Ali GAM, Gupta VK, Makhlouf ASH, Shahryari-ghoshekandi R, Nadagouda MN, Sillanpää M, Megiel E. The role of nanomaterials as effective adsorbents and their applications in wastewater treatment. J Nanostruct Chem. 2017;7(1):1–14.
32. Fronczak M. Adsorption performance of graphitic carbon nitride-based materials: current state of the art. J Environ Chem Eng. 2020;8(5):104411.
33. Sun S, Liang S. Recent advances in functional mesoporous graphitic carbon nitride (mpg-C 3 N 4) polymers. Nanoscale. 2017;9(30):10544–78.
34. Shen W, An Q-D, Xiao Z-Y, Zhai S-R, Hao J-A, Tong Y. Alginate modified graphitic carbon nitride composite hydrogels for efficient removal of Pb (II), Ni (II) and Cu (II) from water. Int J Biol Macromol. 2020;148:1298–306.
35. Zhao Z, Sun Y, Dong F. Graphitic carbon nitride based nanocomposites: a review. Nanoscale. 2015;7(1):15–37.
36. Jiang L, Yuan X, Pan Y, Liang J, Zeng G, Wu Z, Wang H. Doping of graphitic carbon nitride for photocatalysis: a review. Appl Catal B. 2017;217:388–406.
37. Zheng Y, Lin L, Wang B, Wang X. Graphitic carbon nitride polymers toward sustainable photoredox catalysis. Angew Chem Int Ed. 2015;54(44):12868–84.
38. Ong W-J, Tan L-L, Chai S-P, Yong S-T, Mohamed AR. Surface charge modification via protonation of graphitic carbon nitride (g-C3N4) for electrostatic self-assembly construction of 2D/2D reduced graphene oxide (rGO)/g-C3N4 nanostructures toward enhanced photocatalytic reduction of carbon dioxide to methane. Nano Energy. 2015;13:757–70.
39. Ghazy NM, Ghaith EA, Abou El-Reash Y, Zaky RR, Abou El-Maaty WM, Awad FS. Enhanced performance of hydroxyl and cyano group functionalized graphitic carbon nitride for efficient removal of crystal violet and methylene blue from wastewater. RSC Adv. 2022;12(55):35587–97.
40. Lau VW-H, Moudrakovski I, Botari T, Weinberger S, Mesch MB, Duppel V, Senker J, Blum V, Lotsch BV. Rational design of carbon nitride photocatalysts by identification of cyanamide defects as catalytically relevant sites. Nat Commun. 2016;7(1):12165.
41. Dar SH, Hasan N, Rana M, Fatima A, Andrabi SNS, Ahmedi S, Manzoor N, Javed S. Synthesis and spectral studies of Ni (II) complexes involving functionalized dithiocarbamates and triphenylphosphine: X-ray crystal structure, thermal stability, Hirshfeld surface analysis, DFT and biological evaluation. Inorg Chim Acta. 2023;545:121271.
42. Bandyopadhyay P, Li X, Kim NH, Lee JH. Graphitic carbon nitride modified graphene/NiAl layered double hydroxide and 3D functionalized graphene for solid-state asymmetric supercapacitors. Chem Eng J. 2018;353:824–38.
43. Akaike K, Aoyama K, Dekubo S, Onishi A, Kanai K. Characterizing electronic structure near the energy gap of graphitic carbon nitride based on rational interpretation of chemical analysis. Chem Mater. 2018;30(7):2341–52.
44. Zheng Y, Liu J, Liang J, Jaroniec M, Qiao SZ. Graphitic carbon nitride materials: controllable synthesis and applications in fuel cells and photocatalysis. Energy Environ Sci. 2012;5(5):6717–31.
45. Senthil C, Kesavan T, Bhaumik A, Sasidharan M. N-rich graphitic carbon nitride functionalized graphene oxide nanosheet hybrid as anode for high performance lithium-ion batteries. Mater Res Express. 2018;5(1):016307.
46. Ismael M, Wu Y, Taffa DH, Bottke P, Wark M. Graphitic carbon nitride synthesized by simple pyrolysis: role of precursor in photocatalytic hydrogen production. New J Chem. 2019;43(18):6909–20.
47. Niu P, Zhang L, Liu G, Cheng HM. Graphene-like carbon nitride nanosheets for improved photocatalytic activities. Adv Func Mater. 2012;22(22):4763–70.
48. Alwin E, Kočí K, Wojcieszak R, Zieliński M, Edelmannová M, Pietrowski M. Influence of high temperature synthesis on the structure of graphitic carbon nitride and its hydrogen generation ability. Materials. 2020;13(12):2756.
49. Jorge AB, Martin DJ, Dhanoa MT, Rahman AS, Makwana N, Tang J, Sella A, Corà F, Firth S, Darr JA. H_2 and O_2 evolution from water half-splitting reactions by graphitic carbon nitride materials. J Phys Chem C. 2013;117(14):7178–85.
50. Lau VW-H, Mesch MB, Duppel V, Blum V, Senker J, Lotsch BV. Low-molecular-weight carbon nitrides for solar hydrogen evolution. J Am Chem Soc. 2015;137(3):1064–72.
51. Dai H, Gao X, Liu E, Yang Y, Hou W, Kang L, Fan J, Hu X. Synthesis and characterization of graphitic carbon nitride sub-microspheres using microwave method under mild condition. Diam Relat Mater. 2013;38:109–17.
52. Banerjee S, Chattopadhyaya MC. Adsorption characteristics for the removal of a toxic dye, tartrazine from aqueous solutions by a low cost agricultural by-product. Arab J Chem. 2017;10:S1629–38.
53. Martinson CA, Reddy KJ. Adsorption of arsenic(III) and arsenic(V) by cupric oxide nanoparticles. J Colloid Interface Sci. 2009;336(2):406–11.
54. Hu Q, Liu Y, Gu X, Zhao Y. Adsorption behavior and mechanism of different arsenic species on mesoporous $MnFe_2O_4$ magnetic nanoparticles. Chemosphere. 2017;181:328–36.
55. Peng Q, Guo J, Zhang Q, Xiang J, Liu B, Zhou A, Liu R, Tian Y. Unique lead adsorption behavior of activated hydroxyl group in two-dimensional titanium carbide. J Am Chem Soc. 2014;136(11):4113–6.
56. Asere TG, Stevens CV, Du Laing G. Use of (modified) natural adsorbents for arsenic remediation: a review. Sci Total Environ. 2019;676:706–20.
57. Babaee Y, Mulligan CN, Rahaman MS. Removal of arsenic (III) and arsenic (V) from aqueous solutions through adsorption by Fe/Cu nanoparticles. J Chem Technol Biotechnol. 2018;93(1):63–71.
58. Gupta SK, Chen KY. Arsenic removal by adsorption. J Water Pollut Control Fed. 1978;50(3):493–506.
59. Lafferty BJ, Loeppert RH. Methyl arsenic adsorption and desorption behavior on iron oxides. Environ Sci Technol. 2005;39(7):2120–7.
60. Musumba G, Nakiguli C, Lubanga C, Emmanuel N. Adsorption of lead (II) and copper (II) ions from mono synthetic aqueous solutions using bio-char from *Ficus natalensis* fruits. J Encapsul Adsorpt Sci. 2020. https://doi.org/10.4236/jeas.2020.104004.
61. Srivastava S, Agrawal S, Mondal M. Biosorption isotherms and kinetics on removal of Cr (VI) using native and chemically modified *Lagerstroemia speciosa* bark. Ecol Eng. 2015;85:56–66.
62. Dharmapriya TN, Li D, Chung Y-C, Huang P-J. Green synthesis of reusable adsorbents for the removal of heavy metal ions. ACS Omega. 2021;6(45):30478–87.
63. Kwon J-S, Yun S-T, Lee J-H, Kim S-O, Jo HY. Removal of divalent heavy metals (Cd, Cu, Pb, and Zn) and arsenic (III) from aqueous solutions using scoria: kinetics and equilibria of sorption. J Hazard Mater. 2010;174(1–3):307–13.
64. Okafor P, Okon P, Daniel E, Ebenso E. Adsorption capacity of coconut (*Cocos nucifera* L.) shell for lead, copper, cadmium and arsenic from aqueous solutions. Int J Electrochem Sci. 2012;7(1):2354–12369.

65. Afkhami A, Saber-Tehrani M, Bagheri H. Simultaneous removal of heavy-metal ions in wastewater samples using nano-alumina modified with 2, 4-dinitrophenylhydrazine. J Hazard Mater. 2010;181(1–3):836–44.
66. Yang K, Chen B, Zhu X, Xing B. Aggregation, adsorption, and morphological transformation of graphene oxide in aqueous solutions containing different metal cations. Environ Sci Technol. 2016;50(20):11066–75.
67. Abd-Elhamid A, Kamoun EA, El-Shanshory AA, Soliman HM, Aly H. Evaluation of graphene oxide-activated carbon as effective composite adsorbent toward the removal of cationic dyes: composite preparation, characterization and adsorption parameters. J Mol Liq. 2019;279:530–9.
68. Deng J-H, Zhang X-R, Zeng G-M, Gong J-L, Niu Q-Y, Liang J. Simultaneous removal of Cd (II) and ionic dyes from aqueous solution using magnetic graphene oxide nanocomposite as an adsorbent. Chem Eng J. 2013;226:189–200.
69. Sharma P, Singh AK, Shahi VK. Engineering: selective adsorption of Pb (II) from aqueous medium by cross-linked chitosan-functionalized graphene oxide adsorbent. ACS Sustain Chem Eng. 2018;7(1):1427–36.
70. Khatri N, Tyagi S, Rawtani D. Recent strategies for the removal of iron from water: a review. J Water Process Eng. 2017;19:291–304.
71. Ozcan SG, Satiroglu N, Soylak MJF. Column solid phase extraction of iron (III), copper (II), manganese (II) and lead (II) ions food and water samples on multi-walled carbon nanotubes. Food Chem Toxicol. 2010;48(8–9):2401–6.
72. Frisbie SH, Mitchell EJ. Arsenic in drinking water: an analysis of global drinking water regulations and recommendations for updates to protect public health. PLoS ONE. 2022;17(4): e0263505.
73. World Health Organization. A global overview of national regulations and standards for drinking-water quality. 2021.
74. Tang C, Ling L, Zhang W-X. Pb (II) deposition-reduction-growth onto iron nanoparticles induced by graphitic carbon nitride. Chem Eng J. 2020;387:124088.
75. Fernando MS, Wimalasiri A, Dziemidowicz K, Williams GR, Koswattage K, Dissanayake D, de Silva KN, de Silva RM. Biopolymer-based nanohydroxyapatite composites for the removal of fluoride, lead, cadmium, and arsenic from water. ACS Omega. 2021;6(12):8517–30.
76. Rezvani P, Taghizadeh MM. On using clay and nanoclay ceramic granules in reducing lead, arsenic, nitrate, and turbidity from water. Appl Water Sci. 2018;8(5):131.
77. Nikić J, Tubić A, Watson M, Maletić S, Šolić M, Majkić T, Agbaba J. Arsenic removal from water by green synthesized magnetic nanoparticles. Water. 2019;11(12):2520.
78. Puente-Urbina A, Montero-Campos V. Porous materials modified with Fe_3O_4 nanoparticles for arsenic removal in drinking water. Water Air Soil Pollut. 2017;228:1–13.
79. Fan H, Ma X, Zhou S, Huang J, Liu Y, Liu Y. Highly efficient removal of heavy metal ions by carboxymethyl cellulose-immobilized Fe_3O_4 nanoparticles prepared via high-gravity technology. Carbohydr Polym. 2019;213:39–49.
80. Kango S, Kumar R. Magnetite nanoparticles coated sand for arsenic removal from drinking water. Environ Earth Sci. 2016;75:1–12.
81. Jain R. Recent advances of magnetite nanomaterials to remove arsenic from water. RSC Adv. 2022;12(50):32197–209.
82. Park WK, Yoon Y, Kim S, Yoo S, Do Y, Kang J-W, Yoon DH, Yang WS. Feasible water flow filter with facilely functionalized Fe_3O_4-non-oxidative graphene/CNT composites for arsenic removal. J Environ Chem Eng. 2016;4(3):3246–52.
83. Navarathna CM, Karunanayake AG, Gunatilake SR, Pittman CU Jr, Perez F, Mohan D, Mlsna T. Removal of Arsenic (III) from water using magnetite precipitated onto Douglas fir biochar. J Environ Manage. 2019;250:109429.